THz *in vivo* measurements: the effects of pressure on skin reflectivity

JIARUI WANG,[1] RAYKO I. STANTCHEV,[1] QIUSHUO SUN,[1] TOR-WO CHIU,[2] ANIL T. AHUJA,[3] AND EMMA PICKWELL- MACPHERSON[1,4,*]

[1] *Department of Electronic Engineering, The Chinese University of Hong Kong, Shatin, Hong Kong*
[2] *Division of Plastic Reconstructive and Aesthetic Surgery, Department of Surgery, Chinese University of Hong Kong, Shatin, Hong Kong*
[3] *Department of Imaging and Interventional Radiology, The Chinese University of Hong Kong, Shatin, Hong Kong*
[4] *Department of Physics, Warwick University, Coventry, UK*
** e.pickwell.97@cantab.net*

Abstract: Terahertz (THz) light is non-ionizing and highly sensitive to subtle changes in water concentration which can be indicative of disease. The short THz penetration depth in bio-samples restricts *in vivo* measurements to be in a reflection geometry and the sample is often placed onto an imaging window. Upon contacting the imaging window, occlusion and compression of the skin affect the THz response. If not appropriately controlled, this could cause misleading results. In this work, we investigate and quantify how the applied pressure affects the THz response of skin and employ a stratified model to help understand the mechanisms at play. This work will enable future THz studies to have a more rigorous experimental protocol, which in turn will facilitate research in various potential biomedical applications under investigation.

1. Introduction

Terahertz (THz) radiation (0.1 THz to 10 THz) is currently attracting a lot of interest in biomedical research [1–3]. Based on its unique properties, such as non-invasiveness and high sensitivity to water, it has the potential to be used for *in vivo* medical imaging and diagnosis. For example, THz imaging can evaluate early stage deterioration of diabetic patients' feet [4] making it a promising method for the prevention and treatment of ulceration. Bajwa et al. has detected fluid shifts in edema models in rats using THz radiation [5]. Fan et al. showed that THz imaging of human scars could detect changes in the skin that could not be seen by the naked eye [6]. THz radiation also has potential applications in ophthalmology: recent work has used THz radiation for *in vivo* corneal tissue hydration sensing [7,8]. Work by Sy et al. used THz spectroscopy to observe that cirrhotic liver tissues have a higher water content than their healthy counterparts, and even after dehydrating the tissues there were still differences between the normal and cirrhotic liver tissues indicating that the contrast did not only come from a water content difference but also a structural change [9]. Moreover, as demonstrated by Ashworth *et al.* THz imaging can be used to distinguish between healthy tissues and cancer tissues due to fundamental differences in the optical properties [10]. Later, Oh et al. showed that tumors in excised rat brains can be differentiated from healthy brain tissue [11] and Joseph et al. showed that cross-polarized THz imaging can identify skin cancer [12]. Other studies concentrate on improving the contrast between cancer and healthy tissues which can be achieved by using gold nanoparticles as shown in references [13,14]. A comprehensive review of recent THz studies with potential medical applications can be found in reference [3]. Both *in-vivo* and *ex-vivo* THz imaging are of vital importance to help understand tissue structure and pathological changes. However, all the factors and variables affecting THz imaging need to be better understood before THz can be fully utilized in a clinical setting.

Since THz light is highly attenuated in skin by the high THz absorption of water, *in vivo* measurement of human skin can only be done in a reflection geometry. A quartz window is usually used to aid optical alignment and image registration [15,16]. However, when the skin contacts the window, occlusion and mechanical deformation will occur to the skin's surface. Sun et al. investigated the effects of occlusion [17]: their results showed that the THz response of skin changed most rapidly during the first 5 s of contact with the quartz window due to the induced occlusion and therefore water accumulation in the skin. However, to date there have been no studies of how the contact pressure affects the *in-vivo* THz response of skin. There is however the study of Clarys et al showing that the local hydration capacitance of skin is dependent on pressure [18]. Similarly, an investigation using high frequency ultrasound found that after 10 minutes of applying pressure to the heel, the water content increased in the epidermis [19]. Researchers have measured *in vitro* optical properties of skin under different pressures with a visible-IR spectrophotometer [20] and found that the tissue thickness and optical properties changed significantly under different pressures. We therefore expect that pressure, since it affects skin hydration, will also affect the THz response of skin. Additionally, we intuitively expect the biological background components of skin to become compressed and thus denser under the influence of increased pressure. During an *in vivo* THz measurement, slight pressure is applied when the skin makes contact with the quartz window, and this removes unwanted reflections that would occur if there were any air gap. This inevitably compresses the skin (albeit very slightly if minimal pressure is applied) and mechanical deformation occurs. Applying a vertical pressure to the skin will cause the skin to be compressed in the vertical axis, and it will also cause some effects on the skin horizontally. In this work we focus on quantifying the effects on the vertical skin thickness and the hydration of the skin, as these are most relevant to THz *in vivo* skin imaging. Therefore, while the high water sensitivity of THz radiation is a great advantage for skin imaging, other variables such as contact pressure need to be well investigated before this configuration of THz *in vivo* imaging can be put into medical usage.

Here, we study how contact pressure affects the skin's THz properties during *in vivo* THz measurements. We incorporated a pressure sensor into our THz imaging system and continuously measured a single point on the volar forearm under different applied pressures. We applied a stratified media theory model to better evaluate the skin changes under different pressures: our fitting results indicate a reduction in the stratum corneum (SC) thickness and an increase in the water concentration with increasing pressure. Our work demonstrates the importance of controlling and/or monitoring pressure during THz in vivo measurements and will form the basis of future *in vivo* THz imaging protocols.

2. Method

2.1 Experimental setup and protocol

The study was approved by the Joint CUHK-NTEC Clinical Research Ethics Committee and written informed consent was obtained from all volunteers to partake in the study. A customised Menlo (K15) terahertz time-domain system which measures time-domain pulses reflected by a sample was used for the *in vivo* measurements as illustrated in Fig. 1. Details of the system parameters can be found in reference [6]. A THz pulse is launched from a photoconductive emitter [21] and the beam of radiation is focused on the upper surface of an imaging window where the subjects' area of interest is placed, and the reflected signal is collected on to a photoconductive detector. A piece of aluminium foil was put on the imaging window with a $20 \times 20\text{mm}$ aperture cut to help keep the subject keep the correct position during each measurement. A flat pressure sensor (FSR 402), was sandwiched between the area of interest and the aluminium foil adjacent to the THz spot to indicate the local pressure during the measurement.

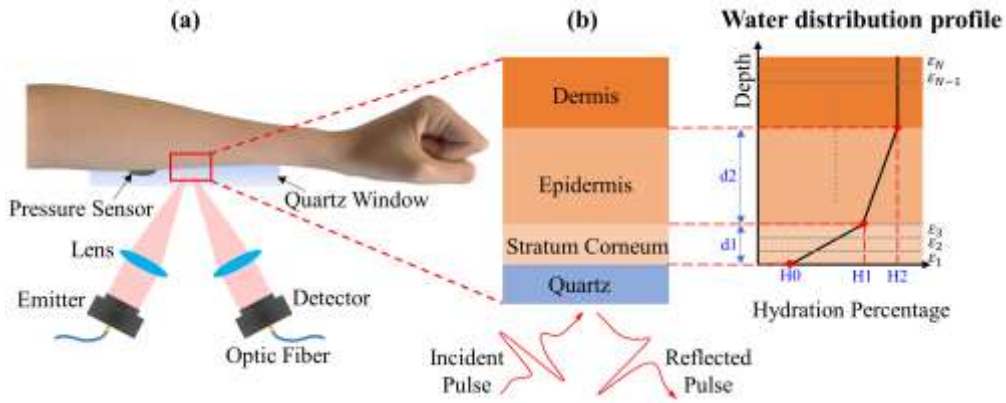

Fig. 1. Experimental setup and stratified media model illustration. (a) The THz beam is focused onto the top interface of the quartz window, and the reflected signal is collected and then detected by a photoconductive antenna. (b) Schematic illustration of the layers within human skin: each layer has a different permittivity. The hydration profile of skin is approximately linear in the SC and epidermis, and constant in the dermis.

Before the experiment, each subject had a 20×20 mm area marked in pen on their volar forearm (2 to 5cm from the edge of the dorsal and the volar forearm and 5 to 10 cm away from the elbow) to make sure each measurement was performed on the same area. Before the experiment, subjects were trained to continuously apply five different pressures (from 1.5N/cm^2 to 3.5N/cm^2). Each measurement recorded one minute of data at a single point at a rate of 4 Hz. To check repeatability, each pressure was measured (for one minute) three times for each subject. The subjects were able to reach the target pressure repeatedly and hold the target pressure for one minute with standard deviation less than 0.1 N/cm^2. Between each measurement of a subject's skin, there was a one hour interval so as to let the area of interest recover back to its normal state and thus eliminate occlusion effects.

This protocol tries to guard against the fact that the structure and properties of skin are very sensitive to position and will vary with hydration. During the one minute measurement the pressure will fluctuate a little but we are able to record this using the pressure sensor.

2.2 Data processing

In this section we outline our method to determine the THz refractive index of skin *in vivo*. In THz time-domain spectroscopy, time-domain measurements containing both the amplitude and phase information from the sample and a reference are acquired. These are then Fourier transformed to the frequency domain and used to recover the complex refractive index. This is done by calculating the reflection coefficients of the sample and reference using the Fresnel equations and Snell's Law. In this work, we obtain a reflection coefficient ratio between the sample and a reference (air). The key equations relevant to our work are given here and more details can be found in references [16,17].

$$M_{meas} = \frac{FFT(E_{sample}(t) - E_{baseline}(t))}{FFT(E_{air}(t) - E_{baseline}(t))} \qquad (1)$$

$$\begin{cases} M_{cal} = \dfrac{r_{qs}}{r_{qa}} = \dfrac{\tilde{n}_q \cos\theta_q - \tilde{n}_s \cos\theta_s}{\tilde{n}_q \cos\theta_q + \tilde{n}_s \cos\theta_s} \cdot \dfrac{\tilde{n}_q \cos\theta_q + \tilde{n}_a \cos\theta_a}{\tilde{n}_q \cos\theta_q - \tilde{n}_a \cos\theta_a} \\ \tilde{n}_a \sin\theta_a = \tilde{n}_q \sin\theta_q = \tilde{n}_s \sin\theta_s \end{cases} \qquad (2)$$

Where $E_{sample}(t)$, $E_{air}(t)$, $E_{baseline}(t)$ are the time domain reflected signals from the sample, air and baseline (discussed below) respectively. $\tilde{n}_s$, $\tilde{n}_a$, $\tilde{n}_q$, θ_s, θ_a, θ_q are the complex refractive index and incident angle of the sample, air and quartz respectively. M_{meas} is the measured ratio, M_{cal} is the calculated reflection coefficient ratio from the relevant optical model; r_{qs} is

the reflection coefficient at the quartz to sample interface and r_{qa} is the reflection coefficient at the quartz to air interface. By fitting the measured data to the calculated data and combining with Snell's law, the refractive index of sample can be extracted.

In our measurement, the first reflection from the air-quartz interface (the baseline in Eq (1)) needs to be removed to eradicate unwanted artefacts [16]. This is achieved by putting another identical quartz window on top of the imaging window to eliminate the second reflection allowing us to record only the baseline and subsequently subtract it. However, the quartz imaging window is not perfectly uniform in thickness and induces errors in the analysis [15]. We use our previously published robust algorithm to eliminate the spatial thickness variation error, laser amplitude noise and pulse shift errors [16]. When applying pressure to the imaging window we may expect the imaging window to shift vertically and possibly become thinner. The pressures we are applying to the quartz window are less than a million times smaller than the Young's modulus of quartz (77 GPa) [22]: a 3 mm piece of quartz would only change by about ~5nm in length. This length scale is negligible in our measurement. Therefore, we still can use the bottom pulse to align the top (sample) pulse and correct for any vertical shift using the algorithm in ref [16].

2.3 THz skin models

Equation (2) in the previous section gives only the average refractive index of a material, since the model assumes the sample is a homogenous material. However, by using more complex optical models we can obtain more information about the sample. For example, stratified media theories can be used to consider skin as a multilayered structure [23,24] and be used to extract information about the different sample layers. Since research has shown that skin has a water concentration gradient [23,25], a more accurate model would take into account how the water concentration changes at different depths. To this end, the permittivity of each individual skin layer is calculated using an effective media model, the Bruggeman model in Eq. (3), consisting of two key components namely water and biological background. The Double Debye model is often used to describe the permittivity of water in the THz regime [26,27]. Here, we use the Debye values for water from reference [27]. The biological background permittivity is left as a parameter to be extracted by the fitting procedure. Research into the structure of skin has shown that the water concentration profile in the stratum corneum can be simplified to increase linearly, followed by a lower gradient in the epidermis and a constant in the dermis [23,25], as shown in Figure 1(b). To accurately account for this, our model consists of 50 individual layers of thickness 2 μm. The relevant equations are shown below:

$$\sum_{i=1}^{J} \eta_i \frac{\varepsilon_i - \varepsilon_{eff}}{\varepsilon_i + 2\varepsilon_{eff}} = 0 \quad (3)$$

$$R_{meas} = \left| M_{meas} \cdot r_{qa} \right|^2 \quad (4)$$

$$R_{cal} = \left| \frac{Z_{skin} - \frac{1}{\cos\theta_{quartz}} \sqrt{\frac{\mu_0}{\varepsilon_0 \varepsilon_{quartz}}}}{Z_{skin} + \frac{1}{\cos\theta_{quartz}} \sqrt{\frac{\mu_0}{\varepsilon_0 \varepsilon_{quartz}}}} \right|^2 \quad (5)$$

Equation (3) is used to calculate the permittivity of skin in each layer and it is frequency-dependence. ε_i is the permittivity of each component (water and biological background in this case), η_i is the volume fraction of each component and combined with the water distribution profile, ε_{eff} is the permittivity of skin in each layer and can be calculated. In Equations (4 and 5), the reflectivity calculation from the measured data and stratified media model is shown. M_{meas} is calculated from the measured data in Eq. (1) and r_{qa} is the reflection coefficient from the quartz-air interface. Z_{skin} is the impedance of skin calculated from the stratified media

model [23] and permittivity of skin in each layer. ε_{quartz} is the permittivity of the quartz window.

In order to understand the mechanical deformation of skin under different pressures, we used the model in the above paragraph to calculate the reflectivity (R_{cal} in Eq. (5)) then fit to our measured reflectivity results R_{meas} [23,24] to evaluate how the various skin parameters change under different pressures. The fitting parameters of our proposed model, shown in blue in Fig. 1(b), are the water concentration in the upper layer of the SC, the epidermis and the dermis; the thicknesses of the SC and the epidermis; and the complex refractive index of the biological background component. By minimizing the differences between the measured and the calculated reflectivity over the frequency range of 0.3 to 0.8THz (the effective bandwidth of our THz-TDS system), these unknown parameters were extracted for each individual pressure.

3. Results and discussion

3.1 THz response of different pressure

Fig. 2(a) shows the THz processed signals of a single point measured under different pressures during the one minute continuous scan. The signals are temporally shifted for clarity. Data thirty seconds after initial contact with the quartz window are plotted here to demonstrate the trend since the occlusion effect is more severe in the first few seconds. Two pressure sensors (as seen in Fig. 2b) were used to help achieve the target pressure consistently during the measurements: the sensor nearer to the elbow gave a real-time readout. The peak to peak value of the processed signal decreased with increasing applied pressure whereas the pulse shape remained the same. To ensure that this phenomenon is due to the pressure and not due to spatial variations of the skin, a 10 × 16 mm area of the volar forearm was also imaged with 2 × 2 mm resolution. Figure 2 (c) is a photograph of the skin during measurement and the results are shown in Fig. 2(d).

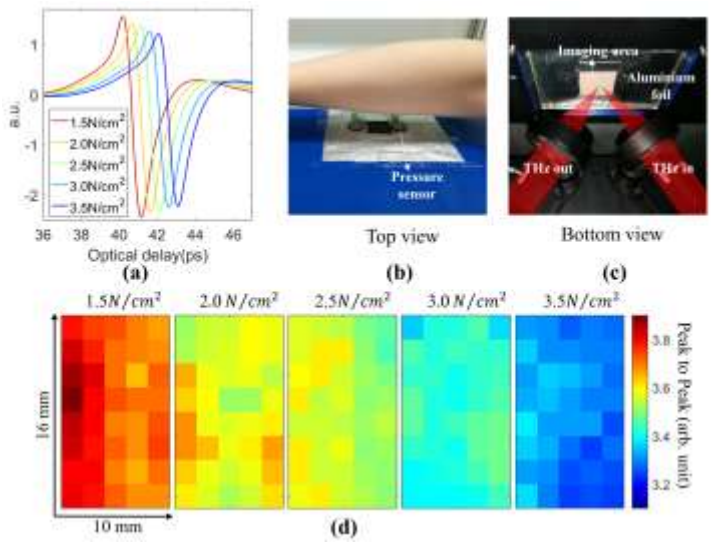

Fig. 2. (a) THz pulse response of skin under different pressures. Photographs of the experimental set up: (b) top view, just before placing the arm on the quartz window and (c) bottom view during measurement (skin is contacting the quartz window) (d) THz images of skin under different pressures.

The pressure value displayed is the target pressure: the actual pressure measured was very close to the target pressure (within 0.1N/cm^{2}of the target value). There is clear reduction of the peak to peak of the processed signal with increasing pressure, verifying this is not due to the spatial inhomogeneity of the skin. Further, in Fig. 2(d) there is an observable decrease of the peak to peak values from left to right of each image. This is due to occlusion by the imaging window, as each image is acquired by raster scanning the THz spot in lines going from up to down and measuring the next line to the right. The duration of the acquisition process for each image was 36 seconds, therefore the left-side of the images are occluded for less time than the right sides, and with increasing occlusion time the peak to peak decreases [17].

3.2 Optical property changes under different pressure

3.2.1 Occlusion time

Fig. 3(a) shows how the reflectivity changes with pressure at 0.6 THz for one subject during a one minute continuous measurement of a single point. The frequency of 0.6 THz is chosen because it is the middle of our spectrum and has the best signal to noise ratio. The data acquisition rate is 4 pulses per second, but for clearer graph plotting, the small circles plotted are the measured reflectivity at 0.6 THz every 2.5 s (i.e. every 10th data point), and the lines are the fitted results of all measured data. The first few seconds of data are removed as this is during unstable pressure when the skin first touches the window. In Fig. 3(a) we see that the reflectivity slightly decreased during the one minute measurement even under the same pressure. Under higher pressures, the reflectivity has a lower starting value than that of lower pressure. The refractive index has similar observation, however, the values are different and the trend is inversed. The change of the values during the one minute measurement is due to the occlusion effect. After the skin makes contact with the imaging window, water starts to accumulate in the SC causing the increase of the refractive index and the decrease of the reflectivity. These results show that occlusion is also a factor that needs to be carefully considered and controlled during *in vivo* measurements.

3.2.2 Reflectivity changes under different pressures

Fig. 3(b) shows the reflectivity at 0.6 THz during a one minute continuous point scan measurement under different pressures for five subjects: the reflectivity decreased with increasing pressure. To increase the signal to noise of our results, we averaged the ten consecutive THz pulses after the skin has been in contact with the imaging window for 30 seconds. The ten THz pulses were acquired in 2.5 seconds and since the skin had already been in contact for 30 seconds, the occlusion affect over these pulses is minimal [17]. Further, each pressure measurement was repeated 3 times to ensure there were no errors caused by the individual's behavior, ie. washing the area under investigation or sweating. The error bar is the standard deviation. From our results, the reflectivity decreased by ~0.02 (over 30%) for the higher pressure and the refractive index increased by ~0.2 (over 10%) with increasing pressure. These results quantify the sensitivity of the skin response to pressure. The most likely reasons for this behavior are that with pressure increasing, the skin is compressed and thus the water concentration and biological density also increase. This idea is also further supported by the proposed fitting model in section 3.3.

3.2.3 Frequency-domain result

Fig. 3(c) and (d) show the reflectivity and refractive index and absorption coefficient from 0.3-0.95 THz respectively for pressures 1.5 N/cm^2 to 3.5N/cm^2, 30 seconds after initial skin contact with quartz window during continuous point scan. The averaged results of three measurements of one subject are plotted. When increasing the applied pressure, the reflectivity decreased and the refractive index increased for all frequencies. No trend was

observed in the absorption coefficient, but it is displayed in Fig. 3 (d) for completeness. Due to the high absorption coefficient of skin (155 cm^{-1} at 0.6 THz), signals reflected from depths of 100 µm will be attenuated by a factor of approximately $e^{-2\times155\times100\times10^{-4}}$ in the frequency range we are measuring. This results in less than 5% of the transmitted signal being reflected back. Therefore in this work we focus on understanding effects in the SC and not deeper in the skin.

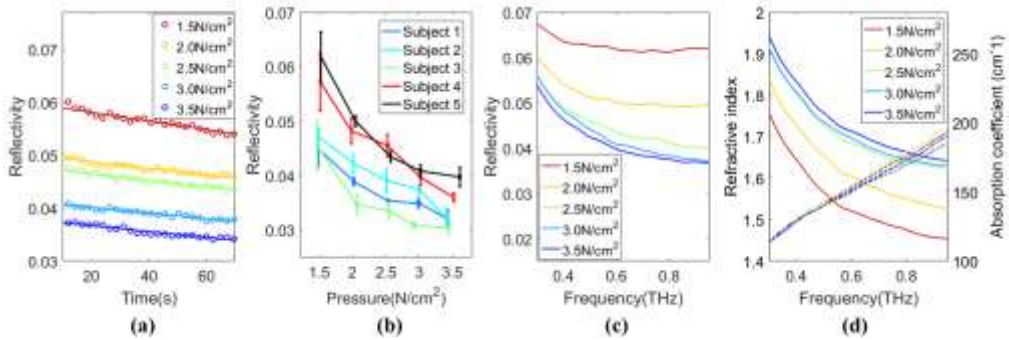

Fig. 3. (a) Reflectivity of skin under different pressures at 0.6 THz during a 1 min continuous point scan measurement. (b) Reflectivity of different subjects under different pressures at 0.6 THz 30 s after skin initially contacts the quartz window. (c) Reflectivity and (d) refractive index (solid lines) and absorption coefficient (dashed lines) of one subject under different pressures from 0.3 THz to 0.95 THz, 30 s after skin initial contact with the quartz window during a one minute continuous point scan. Note that the pressure values displayed are the target pressures.

3.3 Mechanism of pressure effect based on stratified media theory

From the above, we clearly see that the pressure applied to the skin during *in vivo* THz measurements significantly affects the THz response. To determine the corresponding mechanical deformation and property changes we have also applied the stratified media model (see section 2.3 for mathematical details). For each individual, we fit the measured reflectivity with our model and averaged the three fitting results for each pressure. Our results gave repeatable fitting parameters for the three repeats for all pressures and subjects measured. As previously discussed in section 2.3, the skin hydration profile is simplified to be a function of depth which can be represented by the fitting parameters in Figure 1. To understand how the skin changes under different pressures, in Fig. 4(a) we plotted the hydration profile with skin depth, similar to the hydration profile in Figure 1, but for multiple pressures. Fig. 4(a) shows the thickness of the SC and the hydration percentage in the surface of the skin for one subject, with different applied pressures indicated by different colors. The hydration percentage is lower in the outermost part of the SC with a linear increase in it, and it follows a similar trend in the epidermis layer. However, the hydration percentage remains almost constant when it reaches the dermis. From Fig. 4(a), one can see that with increasing pressure the SC slightly decreased in thickness and the hydration percentage increased in the outer layer. Fig 4 (b) shows the refractive index of the dry, biological background component of skin (ie the components not containing water). In reference [23,28], the refractive index of dry skin was measured and found to be frequency independent. To calculate this, we have also assumed that the refractive index of dry porcine skin is frequency independent and deduced the value by using effective medium theory and the stratified media model. We see a clear increase in the real refractive index of the biological component with increasing pressure. Note that the fitting procedures always outputted the imaginary part to be close to zero for all pressures, which was also observed in ref [23,28]. These fitting results support our speculation that both the biological density and water concentration in the SC increase due to the increased compression of the skin.

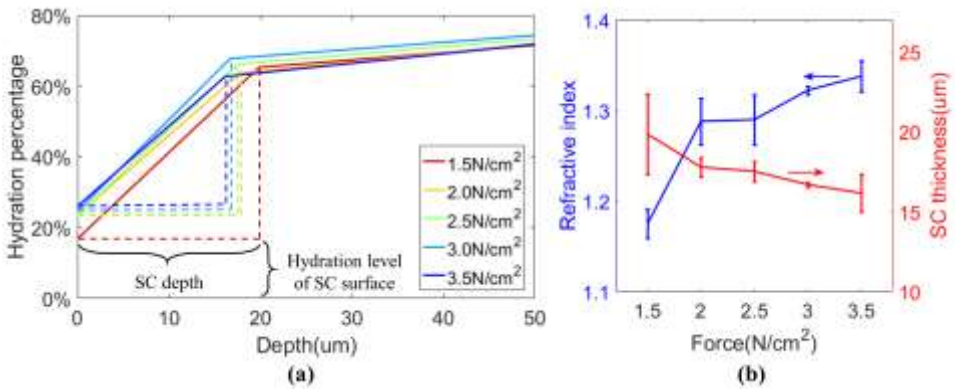

Fig. 4. (a) Water distribution in skin for different pressures. (b) Refractive index of the biological background and calculated SC depth. The error-bars are the standard deviation of three measurements.

4. Conclusion

In this work we focused mostly on how contact pressure affects the THz response during *in vivo* skin imaging. We incorporated two pressure sensors to allow simultaneous measurement of the contact pressure and the THz signals and quantitatively determined the effect of pressure on the skin properties. We observed that the average refractive index can change over 10% when varying the pressure from 1.5 to 3.5N/cm^2. This indicates that THz *in vivo* measurements are very sensitive to the physical force a subject applies. We also analyzed the occlusion effect during one minute under different pressures and found that the occlusion effect leads to a decrease of the reflectivity and an increase in the refractive index with the absolute value being affected by the pressure. To better understand the effect of pressure, we fitted our data to a stratified media model: these modelling results corroborate the hypothesis that as pressure increases, the skin surface is compressed and therefore the water concentration and biological density increase. In summary, this is the first quantitative demonstration that the THz response of skin is very sensitive to contact pressure. This has two implications; firstly, the THz response of skin under different pressures can help understand of skin structure and secondly, it is paramount that the contact pressure is carefully controlled when investigating potential medical applications as inaccurate control of pressure will likely lead to erroneous conclusions.

Funding

This work was partially supported by the Research Grants Council of Hong Kong (project numbers 14206717 and 14201415), the Hong Kong Innovation and Technology Fund (project number ITS/371/16), the Royal Society Wolfson Merit Award and the Hong Kong PhD Fellowship Award.

Acknowledgement

We would like to thank Dr. Xuequan Chen for his advice in data processing and system maintenance support.

Disclosures

The authors declare that there are no conflicts of interest related to this article.

References

1. M. Schirmer, M. Fujio, M. Minami, J. Miura, T. Araki, and T. Yasui, "Biomedical applications of a real-time terahertz color scanner," Biomed. Opt. Express **1(2)**, 354–366 (2010).

2. M. Schwerdtfeger, S. Lippert, M. Koch, A. Berg, S. Katletz, and K. Wiesauer, "Terahertz time-domain spectroscopy for monitoring the curing of dental composites," Biomed. Opt. Express **3(11)**, 2842–2850 (2012).
3. X. Yang, X. Zhao, K. Yang, Y. Liu, Y. Liu, W. Fu, and Y. Luo, "Biomedical Applications of Terahertz Spectroscopy and Imaging," Trends Biotechnol. **34**, 810–824 (2016).
4. G. G. Hernandez-Cardoso, S. C. Rojas-Landeros, M. Alfaro-Gomez, A. I. Hernandez-Serrano, I. Salas-Gutierrez, E. Lemus-Bedolla, A. R. Castillo-Guzman, H. L. Lopez-Lemus, and E. Castro-Camus, "Terahertz imaging for early screening of diabetic foot syndrome: A proof of concept," Sci. Rep. **7**, 1–9 (2017).
5. N. Bajwa, S. Sung, D. B. Ennis, M. C. Fishbein, B. N. Nowroozi, D. Ruan, A. MacCabi, J. Alger, M. A. S. John, W. S. Grundfest, and Z. D. Taylor, "Terahertz Imaging of Cutaneous Edema: Correlation with Magnetic Resonance Imaging in Burn Wounds," IEEE Trans. Biomed. Eng. **64**, 2682–2694 (2017).
6. S. Fan, B. S. Y. Ung, E. P. J. Parrott, V. P. Wallace, and E. Pickwell-MacPherson, "In vivo terahertz reflection imaging of human scars during and after the healing process," J. Biophotonics **10**, 1143–1151 (2017).
7. D. B. Bennett, Z. D. Taylor, P. Tewari, R. S. Singh, M. O. Culjat, W. S. Grundfest, D. J. Sassoon, R. D. Johnson, J.-P. Hubschman, and E. R. Brown, "Terahertz sensing in corneal tissues," J. Biomed. Opt. **16**, 057003 (2011).
8. I. Ozheredov, M. Prokopchuk, M. Mischenko, T. Safonova, P. Solyankin, A. Larichev, A. Angeluts, A. Balakin, and A. Shkurinov, "In vivo THz sensing of the cornea of the eye," Laser Phys. Lett. **15**, (2018).
9. S. Sy, S. Huang, Y. X. J. Wang, J. Yu, A. T. Ahuja, Y. T. Zhang, and E. Pickwell-MacPherson, "Terahertz spectroscopy of liver cirrhosis: Investigating the origin of contrast," Phys. Med. Biol. (2010).
10. P. C. Ashworth, E. Pickwell-MacPherson, E. Provenzano, S. E. Pinder, A. D. Purushotham, M. Pepper, and V. P. Wallace, "Terahertz pulsed spectroscopy of freshly excised human breast cancer," Opt. Express **17**, 12444–12454 (2009).
11. S. J. Oh, S.-H. Kim, Y. Bin Ji, K. Jeong, Y. Park, J. Yang, D. W. Park, S. K. Noh, S.-G. Kang, Y.-M. Huh, J.-H. Son, and J.-S. Suh, "Study of freshly excised brain tissues using terahertz imaging," Biomed. Opt. Express (2014).
12. C. S. Joseph, R. Patel, V. A. Neel, R. H. Giles, and A. N. Yaroslavsky, "Imaging of ex vivo nonmelanoma skin cancers in the optical and terahertz spectral regions," J. Biophotonics (2014).
13. Z. Yang, J. Leon, M. Martin, T. A. Larson, J. Bankson, J. Aaron, and J. Son, "Principle and applications of terahertz molecular imaging," (n.d.).
14. S. J. Oh, J. Kang, I. Maeng, J. Suh, Y. Huh, S. Haam, and J. Son, "Nanoparticle-enabled terahertz imaging for cancer diagnosis," Opt. Express **17**, 3469–3475 (2009).
15. S. Fan, E. P. J. Parrott, B. S. Y. Ung, and E. Pickwell-MacPherson, "Calibration method to improve the accuracy of THz imaging and spectroscopy in reflection geometry," Photonics Res. **4**, A29--A35 (2016).
16. X. Chen, E. P. J. Parrott, B. S. Y. Ung, and E. Pickwell-Macpherson, "A Robust Baseline and Reference Modification and Acquisition Algorithm for Accurate THz Imaging," IEEE Trans. Terahertz Sci. Technol. **7**, 493–501 (2017).
17. Q. Sun, E. P. J. Parrott, Y. He, and E. Pickwell-MacPherson, "In vivo THz imaging of human skin: Accounting for occlusion effects," J. Biophotonics (2018).
18. P. Clarys, R. Clijsen, and A. O. Barel, "Influence of probe application pressure on in vitro and in vivo capacitance (Corneometer CM 825 ®) and conductance (Skicon 200 EX ®) measurements," Ski. Res. Technol. (2011).
19. T. J. Ryan, M. Thoolen, and Y. H. Yang, "The effect of mechanical forces (vibration or external compression) on the dermal water content of the upper dermis and epidermis, assessed by high frequency ultrasound," J. Tissue Viability **11(3)**, 97–101 (2001).
20. E. K. Chan, B. Sorg, D. Protsenko, M. O'Neil, M. Motamedi, and a. J. Welch, "Effects of compression on soft tissue optical properties," IEEE J. Sel. Top. Quantum Electron. **2**, 943–950 (1996).
21. K. Reimann, "Table-top sources of ultrashort THz pulses," Reports Prog. Phys. **70**, 1597–1632 (2007).
22. Z. Peng and S. A. T. Redfern, "Mechanical properties of quartz at the α-β Phase transition: Implications for tectonic and seismic anomalies," Geochemistry, Geophys. Geosystems (2013).
23. D. B. Bennett, W. Li, Z. D. Taylor, W. S. Grundfest, and E. R. Brown, "Stratified media model for Terahertz reflectometry of the skin," IEEE Sens. J. **11**, 1253–1262 (2011).
24. Q. Sun, R. I. Stantchev, J. Wang, E. P. J. Parrott, A. Cottenden, T.-W. Chiu, A. T. Ahuja, and E. Pickwell-MacPherson, "In vivo estimation of water diffusivity in occluded human skin using terahertz reflection spectroscopy," J. Biophotonics e201800145 (2018).
25. R. R. Warner, M. C. Myers, and D. a Taylor, "Electron probe analysis of human skin: determination of the water concentration profile.," J. Invest. Dermatol. (1988).
26. E. Pickwell, B. E. Cole, A. J. Fitzgerald, V. P. Wallace, and M. Pepper, "Simulation of terahertz pulse propagation in biological systems," Appl. Phys. Lett. **84**, 2190–2192 (2004).
27. J. T. Kindt and C. A. Schmuttenmaer, "Far-Infrared Dielectric Properties of Polar Liquids Probed by Femtosecond Terahertz Pulse Spectroscopy †," J. Phys. Chem. **100**, 10373–10379 (1996).

28. Z. D. Taylor, R. S. Singh, D. B. Bennett, P. Tewari, C. P. Kealey, N. Bajwa, M. O. Culjat, A. Stojadinovic, H. Lee, J. P. Hubschman, E. R. Brown, and W. S. Grundfest, "THz medical imaging: In vivo hydration sensing," IEEE Trans. Terahertz Sci. Technol. (2011).